

Original Article

ANN-Based Predictive Modelling for Fused Deposition Modelling: Material Consumption, Tensile Strength & Dimensional Accuracy

Hani Nasuha Hadi Irazman¹, Mohd Sazli Saad^{1*}, Mohamad Ezral Baharudin¹, Mohd Zakimi Zakaria¹, Azuwir Mohd Nor¹, Yuzairi Abdul Rahim¹

¹Faculty of Mechanical Engineering & Technology, University Malaysia Perlis, Pauh Putra Campus, Arau, Perlis, Malaysia.

*Corresponding Author : sazlisaad@unimap.edu.my

Received: 10 July 2023

Revised: 07 September 2023

Accepted: 05 October 2023

Published: 04 November 2023

Abstract - Conventional modelling approaches fall short of accurately capturing the complexities of Fused Deposition Modelling (FDM). This research proposes an Artificial Neural Network (ANN) model to predict the FDM process's material consumption, tensile strength, and dimensional accuracy. Inputs such as layer height, infill density, printing temperature, and printing speed are considered. A Face-Centered Central Composite Design (FCCCD) with 78 specimens is employed to design experiments (DOE). Material consumption is measured using a densimeter, while tensile strength is determined using a Universal Testing Machine (UTM). The performance of the ANN models is evaluated based on metrics like Mean Squared Error (MSE), Root Mean Squared Error (RMSE), Mean Absolute Error (MAE), Mean Absolute Percentage Error (MAPE), and coefficient of determination (R^2). The optimal ANN structure for material consumption prediction is found to be 4-19-14-1, achieving a low MSE of 0.00096. For tensile strength prediction, the best ANN structure is determined as 4-16-15-12-1 with an MSE of 0.005274145. Furthermore, dimensional accuracy is successfully captured using a 4-12-12-11-1 network configuration, which attains the lowest overall MSE of 0.002898. The proposed ANN model provides accurate predictions for material consumption, tensile strength, and dimensional accuracy in the FDM process. This study contributes to the optimization and understanding of FDM manufacturing processes through the utilization of optimized network architectures. The findings demonstrate the efficacy of the ANN model in improving FDM process control and performance.

Keywords - Fused Deposition Modelling, Artificial Neural Network, Process modelling, Face-Centered Central Composite Design, Response surface methodology.

1. Introduction

Artificial Neural Networks (ANN) models have emerged as powerful models capable of recognizing patterns in data and making accurate predictions based on the information they have learned. The increasing complexity of manufacturing processes initiated a growing interest in applying ANN models to address these challenges, including the Fused Deposition Modelling (FDM) process. FDM involves the layer-by-layer deposition of a heated thermoplastic material to create a final product. FDM is widely used in prototyping small-scale products due to its accessibility, versatility, and affordability. Achieving mechanically robust, precise, and sustainable 3D-printed parts hinges on discerning the optimal printing parameter synergy for efficient material utilization. [1]. In recent years, there has been a growing interest in optimizing printing parameters to enhance the quality of 3D-printed products. Johansson's 2016 study [2] explored this topic, focusing on improving tensile properties and layer bonding in 3D-printed objects. The findings from this research

highlighted the significant influence of key parameters such as layer height, infill density, printing speed, and printing temperature on the printed objects' overall quality and structural integrity. This emphasis on parameter optimization is further supported by the work of Nguyen et al. in 2020 [3], where researchers identified optimal printing parameters for achieving enhanced tensile strength, reduced printing time, and minimized material consumption. Layer height, infill density, printing speed, and printing temperature were consistently recognized as primary considerations in optimizing both material usage and dimensional accuracy.

This collective body of research [1, 3-6] underscores the positive correlation between extended printing durations, increased material utilization, and improved mechanical strength, particularly in terms of tensile strength. In the context of FDM, the intricate relationship between material consumption, tensile strength, and dimensional accuracy becomes increasingly apparent. Achieving a balance among



these factors requires a comprehensive understanding of how various process parameters interact and impact the final product. Traditionally, modelling FDM process parameters relied on conventional techniques, including linear regression [7], [8]. However, these methods often fell short of capturing the complexity of non-linear data patterns [9]. Recent advancements in artificial intelligence have led to the adoption of unconventional models such as ANN for process parameter modelling. Inspired by the brain's functional organization, ANN models are trained on available data to identify patterns and generate accurate predictions [10].

A comparative study conducted by Mohamed et al. in 2016 [11] demonstrated the superior predictive performance of ANN models over conventional fractional factorial models, as indicated by higher R^2 values. Similar results were obtained by Lyu et al. in 2019 [12], who compared ANN models to multivariate linear regression and support vector regression, highlighting the limitations of the latter two methods for accommodating multiple process parameters. Furthermore, Deshwal et al. (2020) [4] compared the performance of three hybrid models-Genetic Algorithm-Response Surface Methodology (GA-RSM), Genetic Algorithm-Artificial Neural Network (GA-ANN), and Genetic Algorithm-Adaptive Neuro-Fuzzy Interface System (GA-ANFIS)-in predicting multiple process parameters and tensile strength. Among these models, the GA-ANN model demonstrated the highest accuracy, reaching a remarkable 99.89%.

These findings underscore the importance of employing precise predictive models, such as ANN models, to identify the optimal combination of FDM process parameters effectively. While previous research has demonstrated the effectiveness of ANN models in process modelling, a significant unresolved issue pertains to determining the optimal ANN architecture. This architecture encompasses essential elements, including the number of hidden layers, neurons within each layer, and the selection of an appropriate activation function. Surprisingly, no universally recommended configuration for hidden layers and neurons exists to ensure maximum accuracy in process modelling. Instead, researchers often rely on trial-and-error methods or their existing knowledge when structuring their models [13].

These methods, although somewhat successful, may neglect alternative configurations that could potentially yield even more precise models. This research aims to address this notable gap by identifying the optimal ANN structure capable of outperforming existing models in accurately predicting material consumption, tensile strength, and dimensional accuracy within the FDM process. A series of network models will undergo training to achieve this objective, followed by a comprehensive evaluation using key performance metrics, such as R^2 , MSE , $RMSE$, MAE , and $MAPE$. The focus of this study will center on the input parameters of layer height, infill density, printing speed, and printing temperature.

2. Methodology

2.1. Specimen Design and Material

The specimen used in this study adhered to the International Standard ISO/ASTM D638 Type IV shown in Figure 1, designed using CATIA V5 software. The specimens were printed using Polylactic acid plus (PLA+), with properties shown in Table 1. The Ender 3 V2 3D printer was selected for fabricating the specimen.

2.2. Process Parameter

The process parameters were configured within Cura, an open-source slicing software commonly employed for 3D printing preparations. Cura provided a versatile range of options for setting these parameters before slicing the model into layers, rendering it compatible with most 3D printers. In accordance with insights gleaned from prior research [3], [2], four of the most widely recognized and influential process parameters were selected: layer height, infill density, printing temperature, and printing speed. These choices were made to align with established practices. Concerning the remaining process parameters, their default settings in Cura were retained. Layer height, a crucial parameter in achieving the desired print resolution, was defined as each printed layer's thickness.

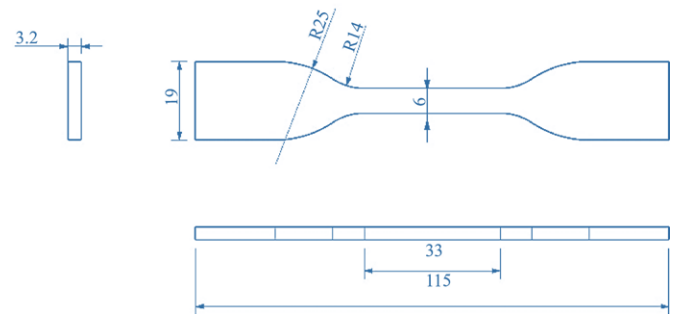


Fig. 1 Dimension ISO/ASTM D638 type IV

Table 1. Properties of polylactic acid plus (PLA+)

Description	Value
Printing temperature	200-230°C
Tolerance	±0.02mm
Printing speed	50-100mm/s
Platform temperature	60-80°C
Diameter	1.75 mm
Melt flow rate	7-9g/10min

As outlined in Buj-Corral et al. 2019 [15], for thermoplastic materials, the recommended range for layer height (h) was generally defined as 0.5 times the nozzle diameter (d) for the lower limit and 0.8 times the nozzle diameter (d) for the upper limit. With the Ender 3 V2's equipped nozzle diameter of 0.4 mm, the minimum and maximum layer heights were calculated using Equation (1)

and Equation (2). Consequently, the minimum layer height was calculated to be 0.2 mm, while the maximum layer height was determined to be 0.32 mm. The quantity of material deposited to fill the boundaries of the printed specimen, known as infill density, was set within a range of 20% to 80%, as recommended by previous studies [3], [14], [15], [16]. In terms of printing temperature, often referred to as nozzle temperature, its optimal value depends on the specific material and printer in use. For PLA+, as indicated in Table 1, the recommended temperature range falls between 200-230°C. In order to determine the most suitable temperature range for the given material and the Ender 3 V2 printer, a temperature tower test was conducted. Figure 2 provides a visual representation of the test results, showing minimal stringing and a smoother surface within the temperature range of 185°C to 215°C.

Consequently, this study's chosen printing temperature range was established as 185°C to 215°C. Printing speed, denoting the rate at which the extruder head moves during the printing process, plays a pivotal role. While Table 1 recommends a manufacturer-recommended range of 50 mm/s to 100 mm/s, recent research on PLA+ has explored a more accelerated printing speed of 150 mm/s [4], [17]. A pragmatic approach was adopted to account for potential outliers and variations in the data, and the selected range for printing speed was extended from 50 mm/s to 150 mm/s. This wider range was chosen to encompass the diversity of printing conditions and accommodate the higher speeds observed in contemporary PLA+ printing studies.

2.3. Design of Experiment

The experimental design followed a systematic approach, integrating Response Surface Methodology (RSM) with a Full Factorial Central Composite Design (FCCD) using Design-Expert software. RSM-FCCD, recognized for its efficacy in optimizing processes or products, delves into identifying the crucial factors influencing the response and their intricate interactions. Design-Expert software emerged as the ideal tool for this purpose, equipped with a user-friendly interface, advanced statistical analysis capabilities, and various graphical representations to streamline the process and enhance accuracy. In the context of this study, the four key process parameters were categorized into three levels: a strategic decision to account for the anticipated non-linear response, as detailed in Table 2.

The experiment proceeded with a full factorial design comprising three factorial points that systematically tested all feasible combinations of factors at the selected levels, and each was replicated three times. Expanding on this, six central points were introduced into the design, carrying out six replications to gauge error variation while maintaining an average level across all factors. To further refine the analysis, three axial points were strategically introduced. These axial points underwent three replications each, operating at the extreme levels of one factor while keeping all other factors at

their average values. This meticulous design yielded a total of 78 specimens to be printed, as outlined in Table 3.

2.4. Fabrication and Experimental Setup

In alignment with the inputs from Table 3, a total of 78 samples were produced using the Ender 3 V2 3D printer. Comprehensive tensile strength tests were executed on all the specimens following this fabrication phase. These tests were carried out using the Shimadzu Universal Testing Machine (UTM), as illustrated in Figure 3, with a standardized testing speed set at 5 mm/min to ensure consistent and accurate results.

$$h \text{ (min)} = 0.5 \times d \tag{1}$$

$$h \text{ (min)} = 0.8 \times d \tag{2}$$

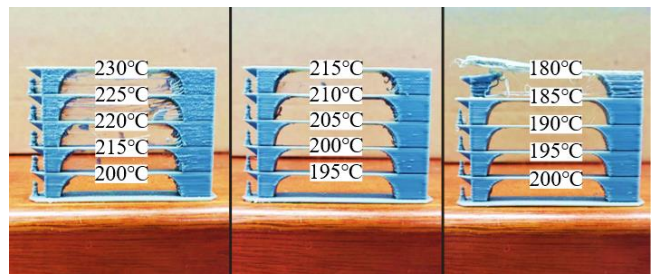


Fig. 2 Temperature tower test

Table 2. Three levels of the four process parameters

Process Parameter	Unit	Level 1	Level 2	Level 3
Layer height	mm	0.2	0.26	0.32
Printing speed	mm/s	50	100	150
Infill density	%	20	50	80
Printing temperature	°C	185	200	215



Fig. 3 Using shimadzu Universal Testing Machine (UTM)

Table 3. FCCCD matrix for process parameters and response

Run	Input				Output		
	Layer Height (mm)	Printing Speed (mm/s)	Infill Density (%)	Printing Temperature (°C)	Weight (g)	Tensile Strength (Pa)	Dimensional Accuracy (mm)
1	0.32	100	50	200	5.23	42.32	0.27
2	0.26	100	50	200	5.03	35.72	0.3
3	0.2	150	80	215	5.86	37.24	0.36
4	0.26	100	20	200	4.44	32.64	0.31
5	0.2	50	80	215	5.65	36.89	0.28
6	0.32	50	80	185	5.56	44.8	0.23
7	0.32	50	20	215	4.88	37.11	0.3
8	0.2	150	20	185	3.94	31.5	0.23
9	0.32	100	50	200	5.24	39.93	0.29
10	0.32	50	20	215	4.91	37.21	0.28
11	0.32	150	80	215	5.6	45.9	0.4
12	0.2	150	80	215	5.68	42.02	0.35
13	0.26	100	50	200	5.11	36.94	0.3
14	0.2	50	20	185	3.98	31.44	0.25
15	0.32	100	50	200	5.25	41.05	0.29
16	0.2	150	80	185	5.67	38.67	0.28
17	0.26	100	50	185	5.07	37.85	0.25
18	0.26	100	50	200	5.16	38.58	0.31
19	0.2	50	20	215	3.99	30.36	0.29
20	0.26	150	50	200	5.08	36.13	0.32
21	0.2	150	20	215	3.97	29.46	0.35
22	0.26	100	50	200	5.1	36.36	0.3
23	0.2	150	80	185	5.6	40.11	0.29
24	0.2	150	20	215	3.93	29.14	0.37
25	0.32	50	80	185	5.47	41.4	0.26
26	0.32	150	80	215	5.58	42.89	0.39
27	0.32	150	20	215	4.74	37.4	0.38
28	0.2	150	20	215	3.91	29.04	0.35
29	0.26	100	20	200	4.36	33.19	0.27
30	0.26	100	50	215	5.16	36.93	0.34
31	0.26	100	80	200	5.84	43.25	0.33
32	0.32	150	20	215	4.86	38.3	0.37
33	0.32	50	80	215	5.59	43.88	0.27
34	0.32	50	20	185	4.82	42.06	0.23
35	0.26	100	50	185	5.08	33.51	0.28
36	0.32	150	20	185	4.66	39.16	0.26
37	0.26	100	80	200	5.82	40.68	0.33
38	0.2	50	80	185	5.62	37.96	0.24
39	0.32	150	80	215	5.58	43.37	0.38
40	0.2	50	80	215	5.86	39.16	0.26
41	0.32	150	80	185	5.47	46.71	0.3
42	0.32	50	20	185	4.78	42.99	0.22
43	0.2	100	50	200	4.87	35.6	0.25
44	0.26	100	50	200	5.18	39.4	0.27
45	0.32	50	80	185	5.67	44.27	0.24
46	0.2	100	50	200	4.85	32.9	0.26
47	0.26	100	20	200	4.44	35.5	0.27
48	0.32	50	20	215	4.92	40.82	0.27
49	0.2	50	80	185	5.71	40.64	0.24

50	0.26	100	50	200	5.14	40.47	0.29
51	0.32	150	20	185	4.64	40.55	0.28
52	0.2	50	80	215	5.7	40.05	0.27
53	0.26	50	50	200	5.21	39.73	0.26
54	0.26	150	50	200	5.14	39.23	0.31
55	0.2	100	50	200	5.1	36.79	0.28
56	0.26	100	50	215	5.44	41.25	0.35
57	0.26	100	50	185	5.3	39.85	0.27
58	0.26	100	50	215	5.43	40.88	0.34
59	0.26	50	50	200	5.2	41.31	0.23
60	0.2	150	20	185	3.91	31.35	0.25
61	0.2	50	80	185	5.74	39.77	0.25
62	0.2	150	80	185	5.7	41.8	0.27
63	0.32	150	80	185	5.49	47.63	0.29
64	0.2	50	20	185	3.94	32.51	0.22
65	0.2	150	80	215	5.84	42.86	0.37
66	0.2	50	20	185	3.96	32.14	0.24
67	0.32	150	80	185	5.46	45.93	0.3
68	0.2	50	20	215	4.02	31.81	0.28
69	0.32	50	80	215	5.76	47.58	0.31
70	0.32	150	20	185	4.63	39.28	0.28
71	0.26	50	50	200	5.19	38.79	0.26
72	0.2	150	20	185	3.88	30.65	0.23
73	0.32	150	20	215	4.86	40.87	0.36
74	0.26	100	80	200	5.67	44.7	0.29
75	0.26	150	50	200	4.93	39.07	0.3
76	0.32	50	80	215	5.66	47.08	0.31
77	0.2	50	20	215	3.97	32.4	0.28
78	0.32	50	20	185	4.79	44.05	0.21

2.5. Artificial Neural Network

In the attempt to develop precise predictive models, a comprehensive study was conducted employing ANN models. The primary objective was to investigate a range of network architectures and evaluate their performance by measuring the *MSE* and *R²*. A total of nine ANN models were meticulously trained, each encompassing single, double, and triple hidden layers, as depicted in Figure 4.

In adherence to Figure 5, the number of neurons within each layer was capped at 20 to optimize computational resources. This constraint facilitated the examination of all 1770 possible network configurations for every response variable. Before the commencement of training, the collected data underwent a normalization procedure, followed by their division into three distinct partitions: training (70%), validation (15%), and testing (15%). The Levenberg-Marquardt algorithm was chosen as the designated training algorithm for the networks. The performance assessment of each model hinged upon the comparison of *MSE* and the *R²* across the 1770 generated network structures for each response variable. Models exhibiting lower *MSE* values and *R²* values approaching 1 were deemed superior in terms of

accuracy.

The most effective architecture for each response variable was earmarked from the cohort of trained networks for future analysis. Ultimately, out of the nine selected architectures, the ANN model with the highest *R²* and the lowest *MSE* for each response variable was singled out as the optimal predictive model structure.

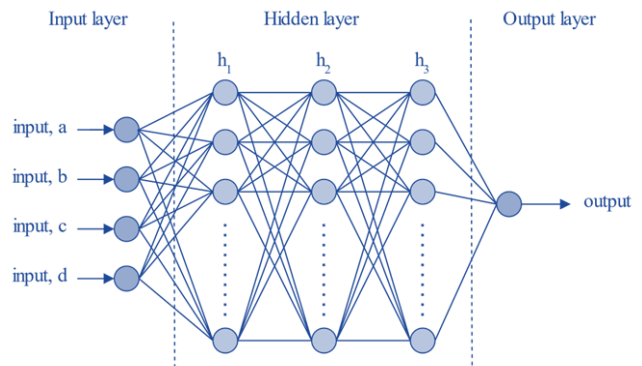


Fig. 4 ANN model structure

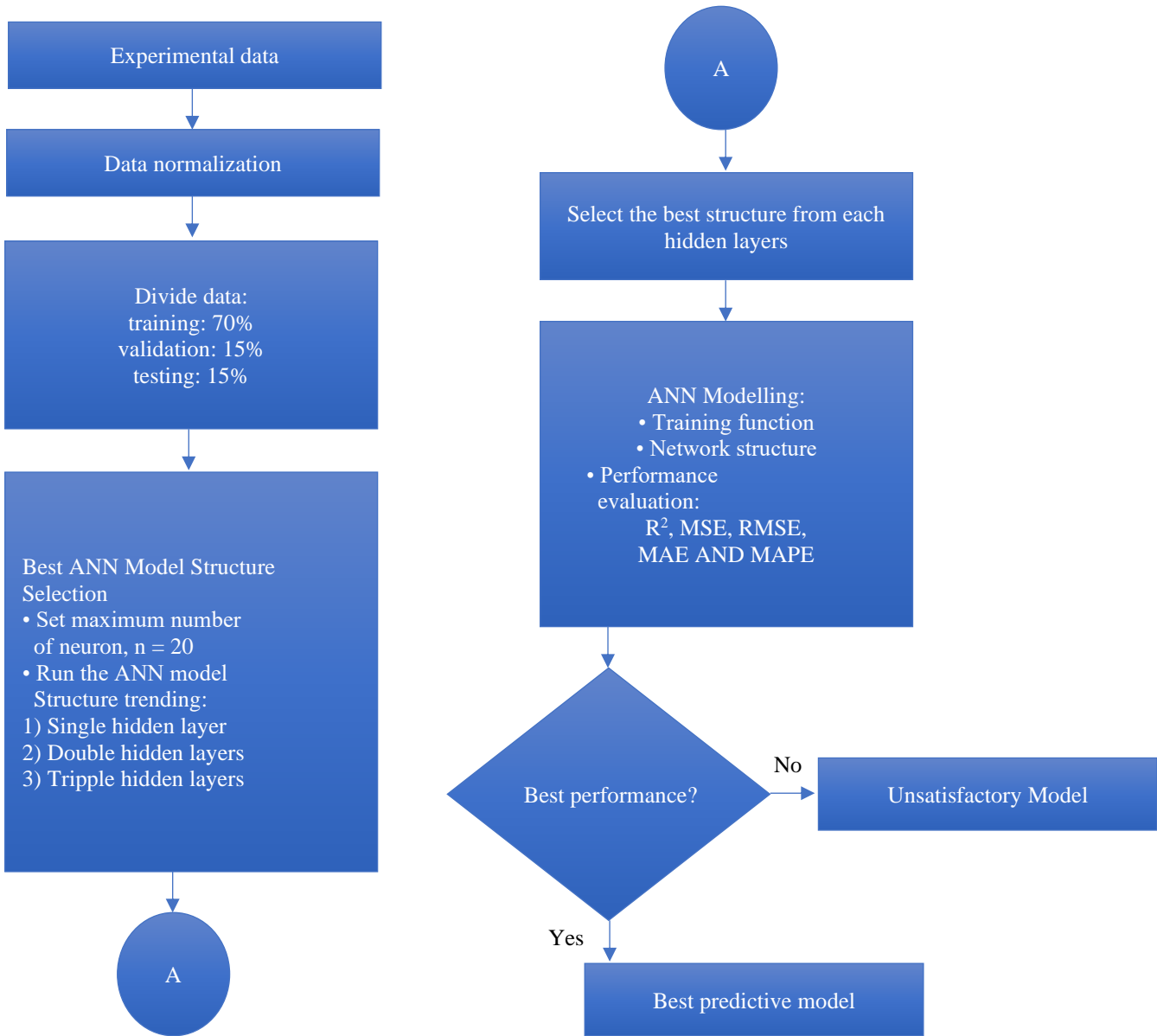


Fig. 5 Flowchart of ANN model development

3. Results and Discussion

3.1. Experimental Results

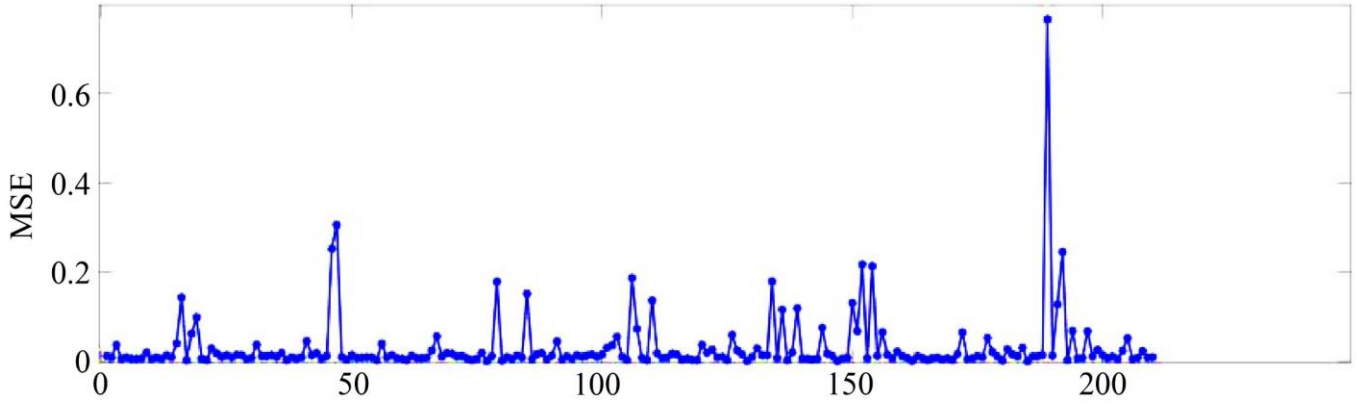
The process parameters for all 78 specimens were set using the slicing software Cura and subsequently executed on the Ender 3 V2 3D printer. Following the printing phase, a comprehensive series of tensile tests on these specimens were conducted, utilizing the Shimadzu Universal Testing Machine (UTM).

The resulting tensile test data were then carefully collected and input into the Design-Expert software for a thorough analysis. This analysis yielded a significant finding, as indicated by the strikingly low p-value, which registered at

less than 0.0001. This high level of statistical significance underscores the robustness and credibility of the model, further affirming the validity of the research outcomes.

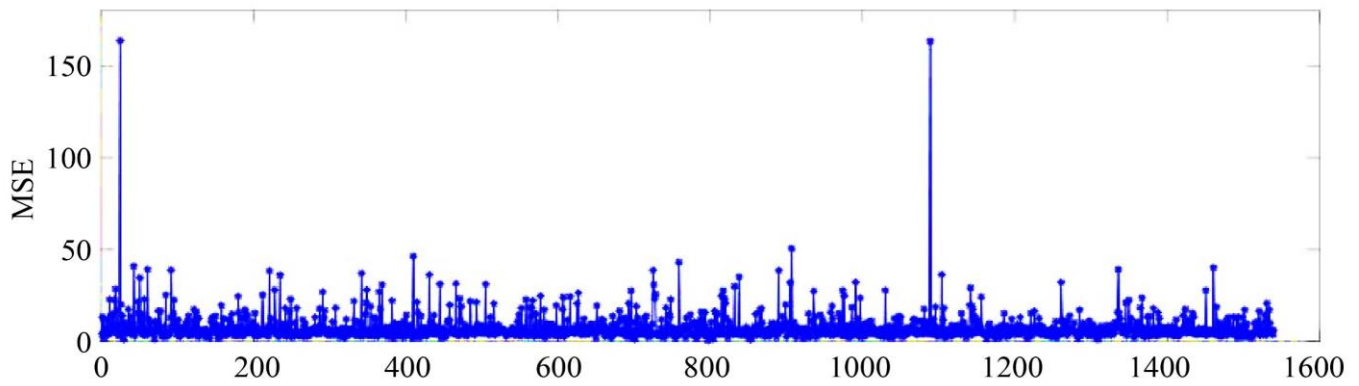
3.2. ANN Results

The generation of ANN model structures involved identifying neuron numbers within hidden layers with the highest accuracy based on the lowest *MSE*, as depicted in Figure 6 for material consumption, Figure 7 for tensile strength, and Figure 8 for dimensional accuracy. Based on the criteria of lowest *MSE* and highest coefficient of determination (R^2), a total of nine ANN model structures were selected, encompassing three structures for each response.



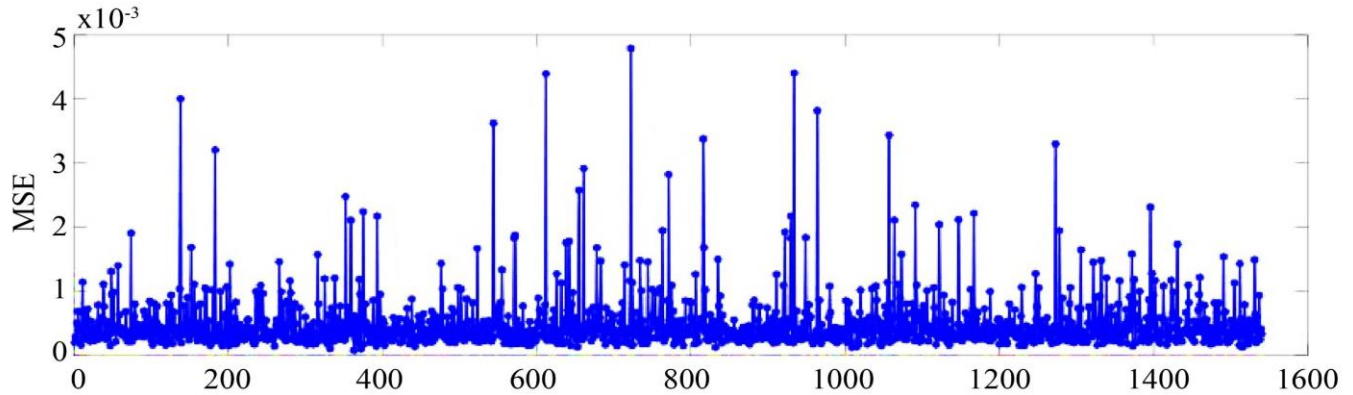
Number of hidden layer neurons for two hidden layer network

Fig. 6 Number of hidden layer neurons against MSE for material consumption



Number of hidden layer neurons for three hidden layer network

Fig. 7 Number of hidden layer neurons against MSE for tensile strength



Number of hidden layer neurons for three hidden layer network

Fig. 8 Number of hidden layer neurons against MSE for dimensional accuracy

Table 4. ANN structures for material consumption

No	Structure	R^2	MSE
1	4-11-1	0.997365	0.002206
2	4-19-14-1	0.998615	0.001391
3	4-10-6-2-1	0.998451	0.001087

Table 5. ANN structures for tensile strength

No	Structure	R^2	MSE
1	4-4-1	0.920185	2.047567
2	4-15-10-1	0.980521	0.999035
3	4-16-15-12-1	0.980607	0.662976

Table 6. ANN structures for dimensional accuracy

No	Structure	R^2	MSE
1	4-1-1	0.96064234	0.00014886
2	4-9-1-1	0.98184033	0.00006857
3	4-12-12-11-1	0.96979763	0.00007049

The selected structures for material consumption are presented in Table 4, while Table 5 showcases the chosen structure for tensile strength, and Table 6 displays the selected structure for dimensional accuracy. Notably, an intriguing observation emerges: the structures pertaining to material consumption exhibit superior performance compared to those associated with tensile strength and dimensional accuracy, as indicated by their higher R^2 values.

This discrepancy might suggest a minimal presence of noise within the collected weight data of the specimen, contributing to a reduced deviation in the output values. It is thereby implied that these structures accurately capture the variations and patterns inherent in the dependent variable, aligning the model's predictions closely with the actual values. However, it is noteworthy that the R^2 values for the tensile strength and dimensional accuracy models remain sufficiently close to 1, indicating their accuracy as well.

On the other hand, in terms of MSE, the ANN structures for dimensional accuracy demonstrate the lowest values compared to the models for material consumption and tensile strength. Nevertheless, the MSE values for the material consumption and tensile strength models are also low, indicating that these models effectively capture the underlying patterns and relationships within the data, with their predictions closely approximating the actual values.

In order to thoroughly evaluate the model's performance, all nine structures were individually examined—the analysis aimed to assess their effectiveness in capturing the underlying patterns and relationships within the data. The obtained results from the modelled networks were meticulously documented and organized for each response, as presented in Table 7, Table 8, and Table 9. Upon reviewing Table 7, it is evident that structure 4-19-14-1 outperformed the other structures in terms of material consumption. This particular structure exhibited the lowest average values for MSE, RMSE, MAE, and MAPE.

Furthermore, it demonstrated the highest R^2 for both training and overall performance. Turning to Table 8, the evaluation of tensile strength reveals that structure 4-16-15-12-1 showcased superior performance.

This specific structure achieved the highest R^2 values for testing and overall while simultaneously attaining the lowest values for MSE, RMSE, MAE, and MAPE in both training and overall assessments. Finally, in Table 9, the examination of dimensional accuracy indicates that structure 4-12-12-11-1 delivered the most favourable outcomes.

It demonstrated the highest R^2 values for testing and overall and the lowest values for MSE, RMSE, MAE, and MAPE in both training and overall evaluations. In summary, through a meticulous analysis of the modelled structures, it becomes evident that specific configurations excelled in capturing and predicting the responses of interest. These findings provide valuable insights into the optimization of the model for material consumption, tensile strength, and dimensional accuracy.

Figure 9, Figure 10, and Figure 11 provide additional visual representations of the comparison between the overall performance metrics for all the ANN models in terms of material consumption, tensile strength, and dimensional accuracy, respectively. Among the analyzed structures, structure 4-19-14-1 with double hidden layers, consisting of 19 and 14 neurons, respectively, demonstrated superior material consumption performance, as shown in Figure 12.

Additionally, for accurate prediction of tensile strength, structure 4-16-15-12-1 with triple hidden layers, comprising 16, 15, and 12 neurons, respectively, was identified as the optimal choice, illustrated in Figure 13. Moreover, for dimensional accuracy, structure 4-12-12-11-1 with triple hidden layers, consisting of 12, 11, and 11 neurons each, exhibited exceptional performance, as depicted in Figure 14.

Table 7. Performance for structures of material consumption

Structure	Function	Training	Validation	Testing	Overall
4-11-1	R^2	0.9958	0.9893	0.98925	0.99192
	MSE	0.000413	0.002948	0.001533	0.000961
	RMSE	0.020323	0.054299	0.039149	0.031
	MAE	1.427573	3.771887	2.96396	2.004907
	MAPE	2.705481	7.347113	7.392791	4.080609
4-19-14-1	R^2	0.995854	0.988584	0.98946	0.991945
	MSE	0.000408	0.002982	0.001503	0.000958
	RMSE	0.020193	0.054608	0.038769	0.030956
	MAE	1.391232	3.756713	2.944581	1.974214
	MAPE	2.599909	7.25051	7.330353	3.9825
4-10-6-2-1	R^2	0.988738	0.988585	0.990512	0.987203
	MSE	0.001114	0.003029	0.001749	0.001498
	RMSE	0.033379	0.055037	0.041824	0.038708
	MAE	2.401556	3.870156	3.239789	2.745707
	MAPE	4.654881	8.03187	9.51716	5.860123

Table 8. Performance for structures of tensile strength

Structure	Function	Training	Validation	Testing	Overall
4-4-1	R^2	0.9958	0.9893	0.98925	0.99192
	MSE	0.000413	0.002948	0.001533	0.000961
	RMSE	0.020323	0.054299	0.039149	0.031
	MAE	1.427573	3.771887	2.96396	2.004907
	MAPE	2.705481	7.347113	7.392791	4.080609
4-15-10-1	R^2	0.995854	0.988584	0.98946	0.991945
	MSE	0.000408	0.002982	0.001503	0.000958
	RMSE	0.020193	0.054608	0.038769	0.030956
	MAE	1.391232	3.756713	2.944581	1.974214
	MAPE	2.599909	7.25051	7.330353	3.9825
4-16-15-12-1	R^2	0.988738	0.988585	0.990512	0.987203
	MSE	0.001114	0.003029	0.001749	0.001498
	RMSE	0.033379	0.055037	0.041824	0.038708
	MAE	2.401556	3.870156	3.239789	2.745707
	MAPE	4.654881	8.03187	9.51716	5.860123

Table 9. Performance for structures of dimensional accuracy

Structure	Function	Training	Validation	Testing	Overall
4-1-1	R^2	0.909147	0.965865	0.877974	0.914883
	MSE	0.005873	0.003045	0.006426	0.005516
	RMSE	0.076633	0.055182	0.080161	0.074267
	MAE	6.083916	4.607907	5.608769	5.78983
	MAPE	6.083916	4.607907	5.608769	5.78983
4-9-1-1	R^2	0.974709	0.944296	0.868739	0.955769
	MSE	0.001679	0.004264	0.007506	0.002898
	RMSE	0.040973	0.065298	0.086638	0.053836
	MAE	3.247345	5.450482	7.082315	4.127118
	MAPE	8.276126	20.35382	19.98784	11.78589
4-12-12-11-1	R^2	0.974709	0.944386	0.868642	0.955769
	MSE	0.053834	0.004257	0.007512	0.002898
	RMSE	0.040973	0.065248	0.08667	0.053834
	MAE	7.079135	5.44625	7.079135	4.126319
	MAPE	8.277185	20.33418	19.97489	11.78178

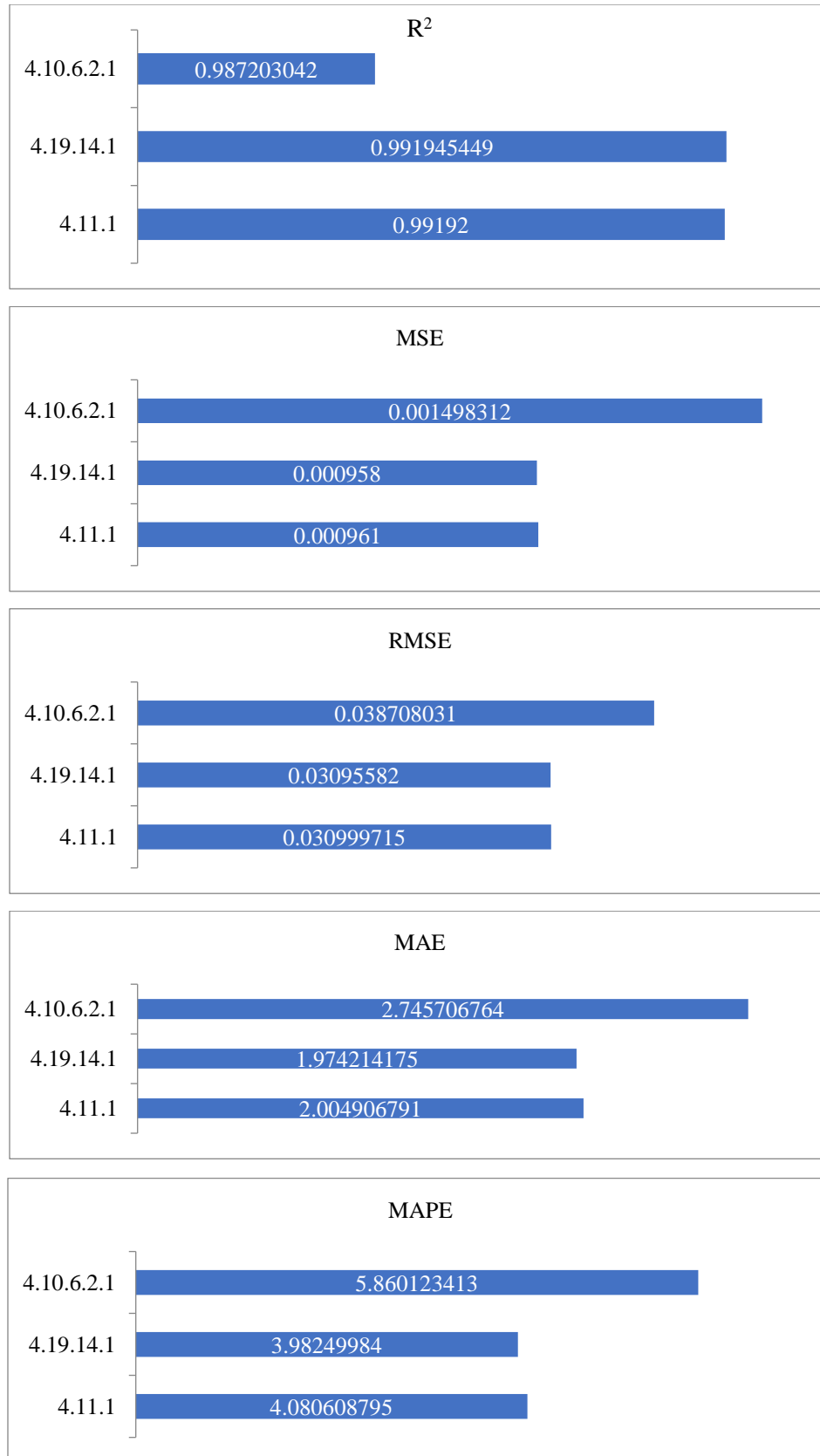


Fig. 9 Performance metrics of ANN models for material consumption

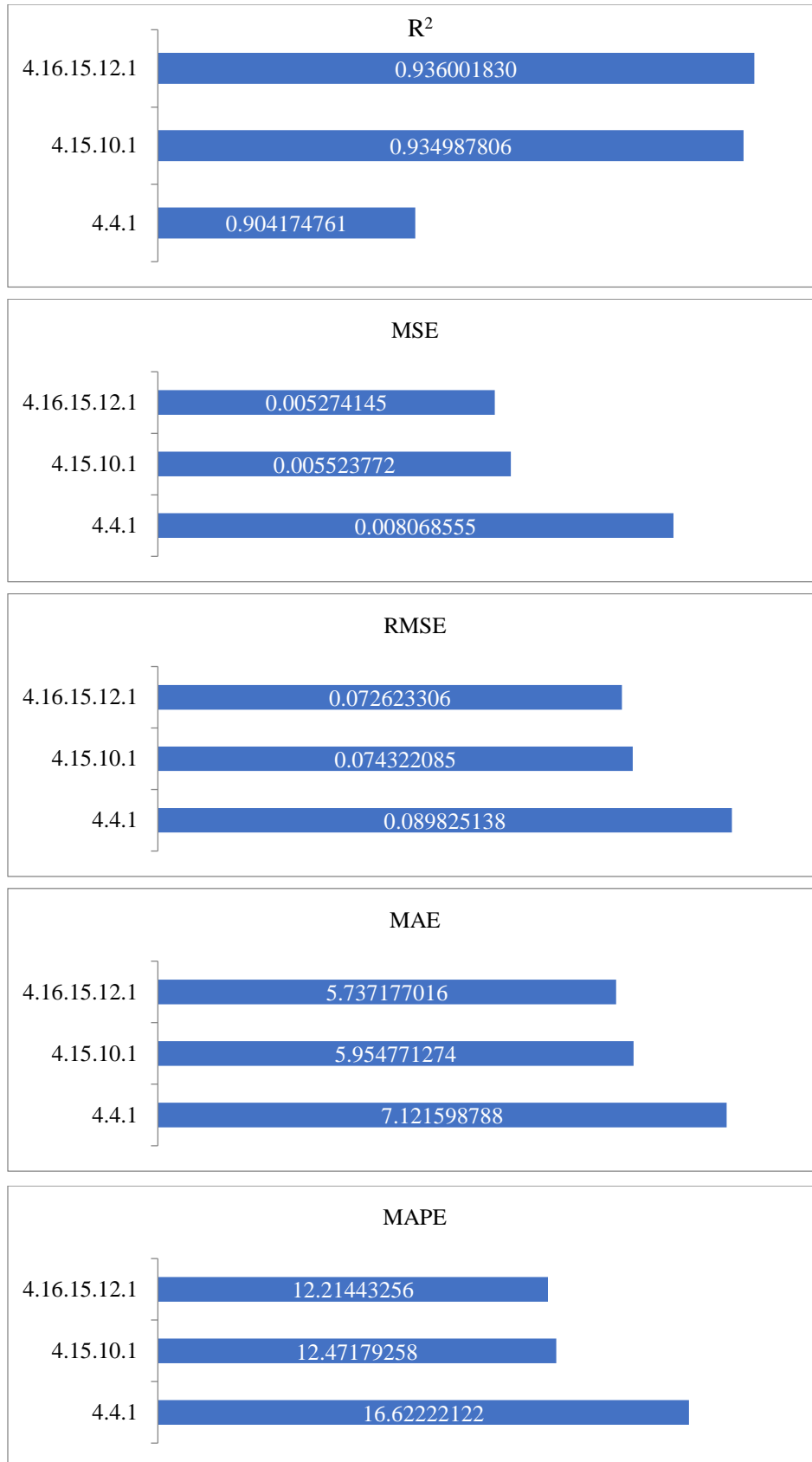


Fig. 10 Performance metrics of ANN models for tensile strength

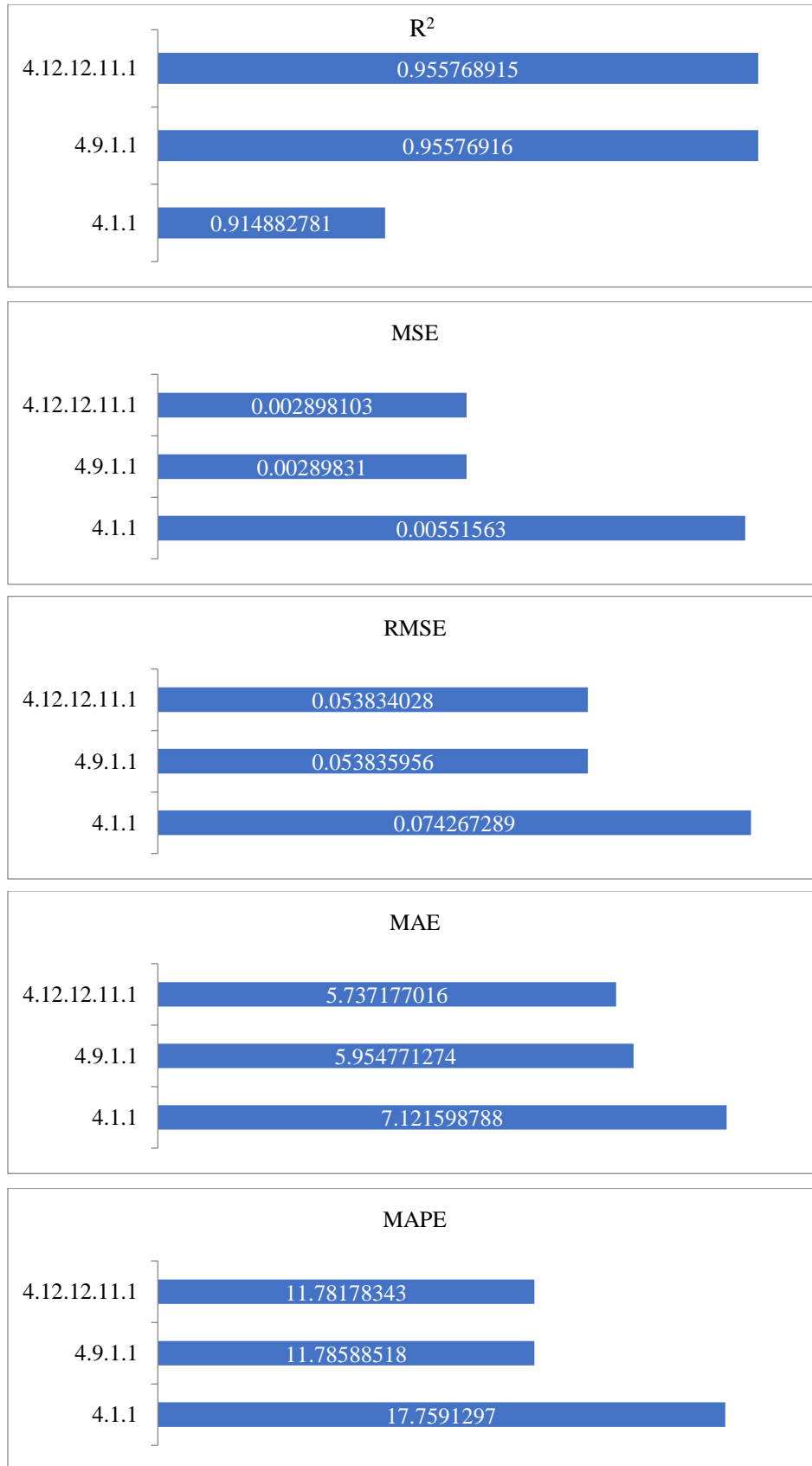


Fig. 11 Performance metrics of ANN models for dimensional accuracy

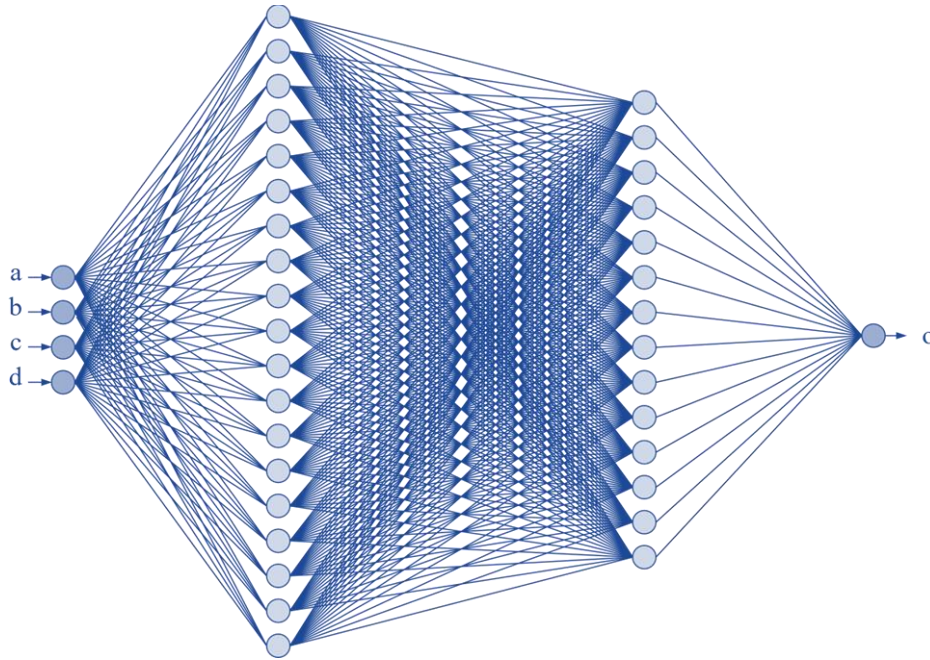


Fig. 12 ANN model structure of 4-19-14-1 for material consumption

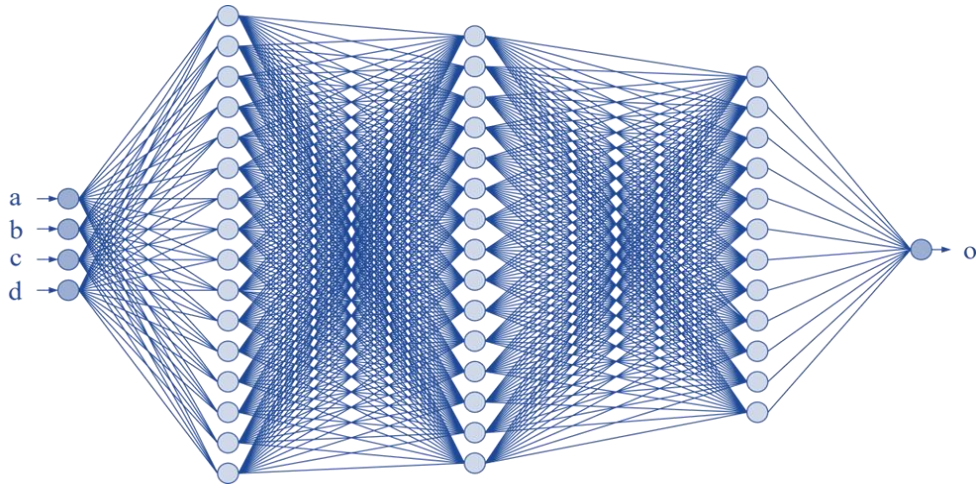


Fig. 13 ANN model structure 4-16-15-12-1 for tensile strength

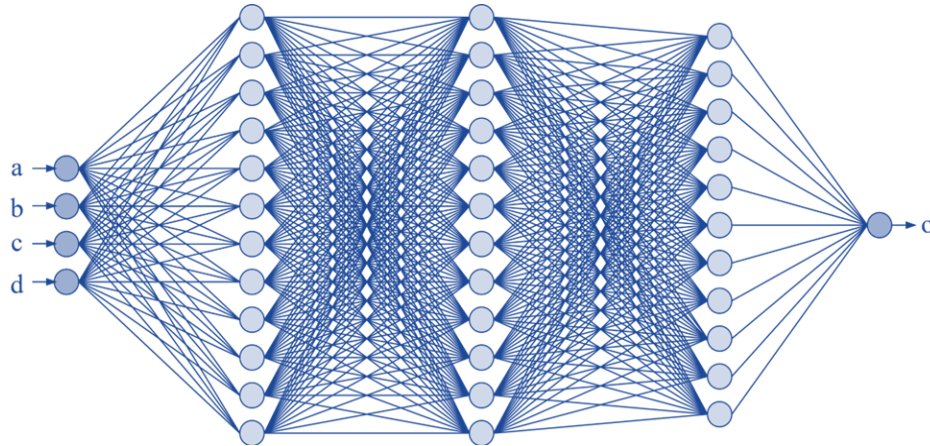


Fig. 14 ANN model structure 4-12-12-11-1 for dimensional accuracy

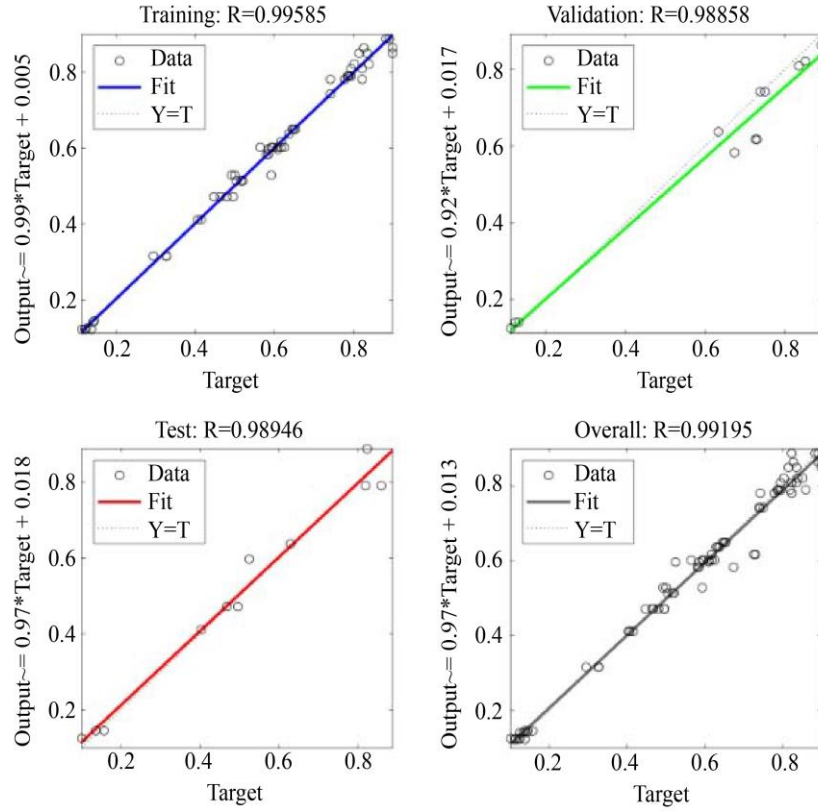


Fig. 15 Linear regression plot of 4-19-14-1 (material consumption)

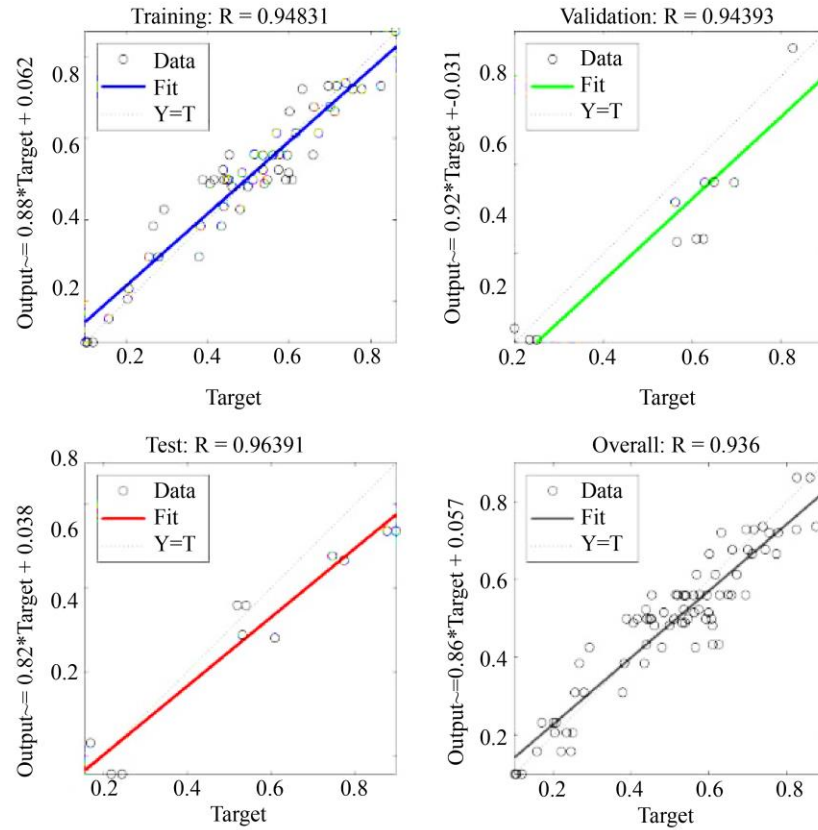


Fig. 16 Linear regression plot of 4-16-15-12-1 (tensile strength)

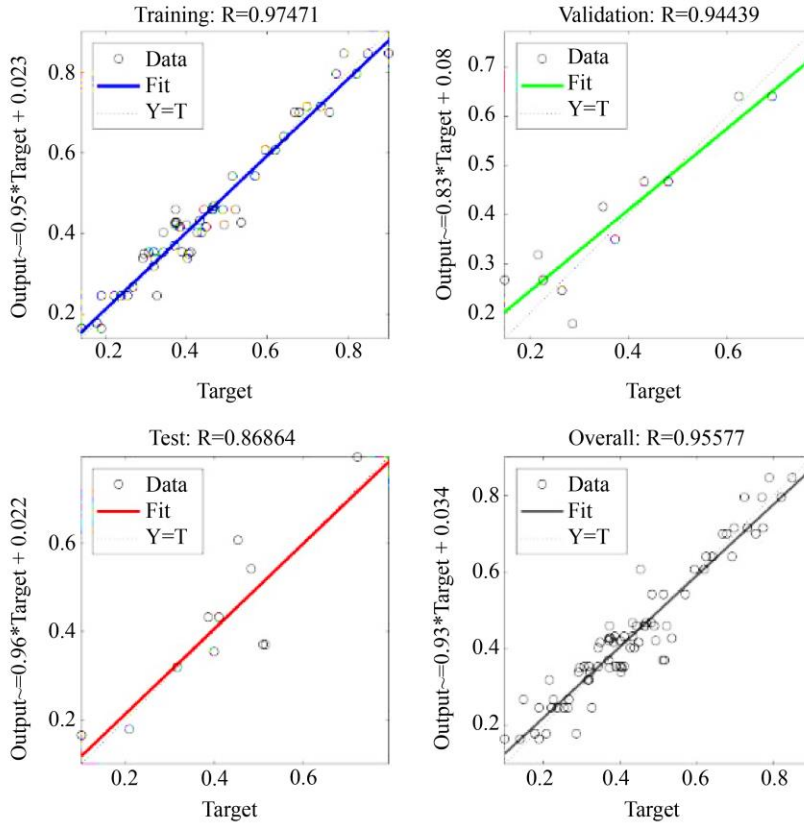


Fig. 17 Linear regression plot of 4-12-12-11-1 (dimensional accuracy)

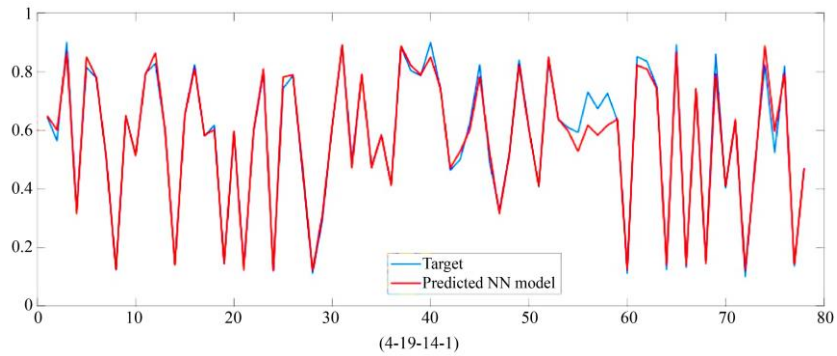


Fig. 18 Overall target and predicted plot for material consumption

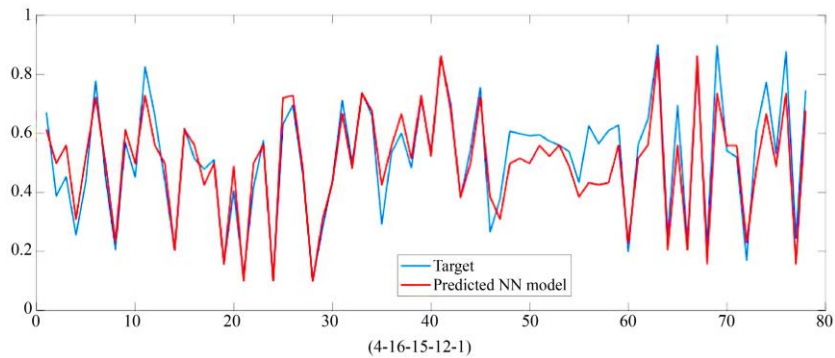


Fig. 19 Overall target and predicted plot for tensile strength

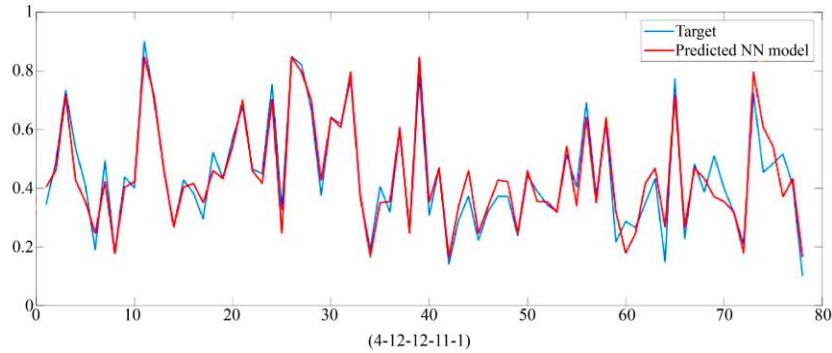


Fig. 20 Overall target and predicted plot for dimensional accuracy

The regression plots provide valuable insights into the relationship between the independent and dependent variables. Notably, the regression line for the material consumption model (Figure 15) displayed a closer fit to the ideal value of 1 compared to the regression lines for the tensile strength model (Figure 16) and the dimensional accuracy model (Figure 17). This discrepancy could potentially be attributed to the presence of noise originating from the collected data for the tensile strength test and dimensional accuracy measurement. Overall, the regression plots for all models indicate that the independent variable holds the potential to explain the observed variations in the dependent variables.

The plotted lines for these models demonstrate a high capability for accurately predicting reactions based on the provided input shown in Figure 18 (material consumption), Figure 19 (tensile strength) and Figure 20 (dimensional accuracy). It is essential to highlight that a discernible discrepancy can be observed among the plotted line of the tensile strength model compared to the models for material consumption and dimensional accuracy. This discrepancy directly corresponds with the comparatively elevated *MSE* value and reduced R^2 exhibited by the tensile strength model. These findings emphasize the efficacy of the selected structures in capturing and predicting the target responses. By leveraging these models, researchers can make more precise predictions and gain valuable insights into material consumption, tensile strength, and dimensional accuracy.

4. Conclusion

In contrast to techniques commonly found in the existing literature, this study has undertaken an extensive exploration of various ANN architectures during the network training process. The primary aim of this research was to predict and optimize process parameters to enhance three critical aspects of FDM printed parts: material consumption, tensile strength, and dimensional accuracy. One notable aspect of this study is the significantly larger number of model architectures generated compared to other methods. This extensive exploration increases the likelihood of discovering a more accurate model than alternative approaches.

By integrating essential input variables, including layer height, infill density, printing temperature, and printing speed, into the ANN models, this study has achieved remarkable results that surpass the performance of conventional techniques outlined in the literature. The ANN models exhibited exceptional predictive capabilities, enabling significant reductions in material consumption, substantial increases in tensile strength, and remarkable improvements in dimensional accuracy for FDM printed parts. The application of the Levenberg-Marquardt algorithm as a training function allows for the simulation of the influence of process parameters on the desired outcome.

This research provides valuable insights into the potential of ANN-based process modelling as a robust approach for predicting and optimizing FDM parameters, thereby improving the overall tensile strength of manufactured parts. The performance evaluation of the ANN models was conducted using a comprehensive set of performance metrics, R^2 , *MSE*, *RMSE*, *MAE*, and *MAPE*. Among the selected ANN models, the structure of 4-19-14-1 for material consumption, 4-16-15-12-1 for tensile strength and 4-12-12-11-1 for dimensional accuracy exhibited the highest degree of agreement between the experimental data and the corresponding predicted values as evidenced by the remarkably low *MSE* values and R^2 closest to 1.

The predictive capabilities of the developed ANN model provide a powerful means of establishing a functional relationship between the input parameters and the output characteristics of the FDM process, making it an effective alternative to traditional analytical and numerical models. The utilization of ANN models holds substantial promise for addressing complex challenges encountered in diverse manufacturing processes.

Further investigations into the architectural aspects of ANN models are warranted to develop even more accurate and precise models, minimizing any potential errors. Implementing ANN models to enhance performance outputs, particularly in industries such as manufacturing, healthcare, automotive, aerospace, and finance, exhibits great potential

for transformative impacts. Nonetheless, it is crucial to acknowledge the limitations associated with ANN models, such as their resource-intensive nature when training larger networks with increased hidden layers and neurons. Striving for superior outcomes necessitates a comprehensive understanding of these limitations and the judicious integration of ANN models with complementary methodologies, including statistical analysis and rule-based systems.

References

- [1] Mark Goudswaard, Ben Hicks, and Aydin Nassehi, "The Creation of a Neural Network Based Capability Profile to Enable Generative Design and the Manufacture of Functional FDM Parts," *The International Journal of Advanced Manufacturing Technology*, vol. 113, pp. 2951-2968, 2021. [[CrossRef](#)] [[Google Scholar](#)] [[Publisher Link](#)]
- [2] Frans Johansson, "Optimizing Fused Filament Fabrication 3D Printing for Durability: Tensile Properties and Layer Bonding," M.S. Dissertation, Blekinge Institute of Technology, Karlskrona, Sweden, pp. 1-88, 2016. [[Google Scholar](#)] [[Publisher Link](#)]
- [3] V.H. Nguyen et al., "Single and Multi-Objective Optimisation of Processing Parameters for Fused Deposition Modelling in 3D Printing Technology," *International Journal of Automotive and Mechanical Engineering*, vol. 17, no. 1, pp. 7542-7551, 2020. [[CrossRef](#)] [[Google Scholar](#)] [[Publisher Link](#)]
- [4] Sandeep Deshwal, Ashwani Kumar, and Deepak Chhabra, "Exercising Hybrid Statistical Tools GA-RSM, GA-ANN and GA-ANFIS to Optimize FDM Process Parameters for Tensile Strength Improvement," *CIRP Journal of Manufacturing Science and Technology*, vol. 31, pp. 189-199, 2020. [[CrossRef](#)] [[Google Scholar](#)] [[Publisher Link](#)]
- [5] Vinaykumar S. Jatti et al., "A Study on Effect of Fused Deposition Modeling Process Parameters on Mechanical Properties," *International Journal of Scientific and Technology Research*, vol. 8, no. 11, pp. 689-693, 2019. [[Google Scholar](#)] [[Publisher Link](#)]
- [6] Carmita Camposeco-Negrete, "Optimization of Printing Parameters in Fused Deposition Modelling for Improving Part Quality and Process Sustainability," *The International Journal of Advanced Manufacturing Technology*, vol. 108, pp. 2131-2147, 2020. [[CrossRef](#)] [[Google Scholar](#)] [[Publisher Link](#)]
- [7] Nikolaos A. Fountas, and Nikolaos M. Vaxevanidis, "Optimization of Fused Deposition Modelling Process Using a Virus-Evolutionary Genetic Algorithm," *Computers in Industry*, vol. 125, 2021. [[CrossRef](#)] [[Google Scholar](#)] [[Publisher Link](#)]
- [8] Balwant Singh, Raman Kumar, and Jasgurpreet Singh Chohan, "Multi-Objective Optimization of the 3D Printing Process Using Genetic Algorithm for Fabrication of Copper Reinforced ABS Parts," *Materials Today: Proceedings*, vol. 48, pp. 981-988, 2022. [[CrossRef](#)] [[Google Scholar](#)] [[Publisher Link](#)]
- [9] Louis Anthony Cox, "Implications of Nonlinearity, Confounding, and Interactions for Estimating Exposure Concentration-Response Functions in Quantitative Risk Analysis," *Environmental Research*, vol. 187, 2020. [[CrossRef](#)] [[Google Scholar](#)] [[Publisher Link](#)]
- [10] Md. Mostafizur Rahman, Abu Reza Md. Towfiqul Islam, and Mashura Shammi, "Emerging Trends of Water Quality Monitoring and Applications of Multivariate Tools," *Water Engineering Modeling and Mathematic Tools*, pp. 271-283, 2021. [[CrossRef](#)] [[Google Scholar](#)] [[Publisher Link](#)]
- [11] Omar A. Mohamed, Syed H. Masood, and Jahar L. Bhowmik, "Investigation of Dynamic Elastic Deformation of Parts Processed by Fused Deposition Modelling Additive Manufacturing," *Advances in Production Engineering and Management*, vol. 11, no. 3, pp. 227-238, 2016. [[CrossRef](#)] [[Google Scholar](#)] [[Publisher Link](#)]
- [12] Jiaqi Lyu, and Souran Manoochchri, "Dimensional Prediction for FDM Machines Using Artificial Neural Network and Support Vector Regression," *Proceedings ASME Design Engineering Technical Conference*, vol. 1, 2019. [[CrossRef](#)] [[Google Scholar](#)] [[Publisher link](#)]
- [13] Izabela Rojek et al., "AI-Optimized Technological Aspects of the Material Used in 3D Printing Processes for Selected Medical Applications," *Materials*, vol. 13, no. 23, pp. 1-19, 2020. [[CrossRef](#)] [[Google Scholar](#)] [[Publisher link](#)]
- [14] Saty Dev, and Rajeev Srivastava, "Experimental Investigation and Optimization of FDM Process Parameters for Material and Mechanical Strength," *Materials Today: Proceedings*, vol. 26, pp. 1995-1999, 2020. [[CrossRef](#)] [[Google Scholar](#)] [[Publisher link](#)]
- [15] Irene Buj-Corral et al., "Influence of Infill and Nozzle Diameter on Porosity of FDM Printed Parts with Rectilinear Grid Pattern," *Procedia Manufacturing*, vol. 41, pp. 288-295, 2019. [[CrossRef](#)] [[Google Scholar](#)] [[Publisher Link](#)]
- [16] Damir Hodzic, and Adi Pandzic, "Influence of Infill Design on Compressive and Flexural Mechanical Properties of FDM Printed PLA Material," *Annals of DAAAM and Proceedings*, pp. 191-200, 2021. [[CrossRef](#)] [[Google Scholar](#)] [[Publisher link](#)]
- [17] Mohammad S. Alsoufi et al., "Influence of Multi-Level Printing Process Parameters on 3D Printed Parts in Fused Deposition Molding of Poly(lactic) Acid Plus: A Comprehensive Investigation," *American Journal of Mechanical Engineering*, vol. 7, no. 2, pp. 87-106, 2019. [[CrossRef](#)] [[Google Scholar](#)] [[Publisher Link](#)]
- [18] Vivek Basavegowda Ramu, "Performance Testing Using Machine Learning," *SSRG International Journal of Computer Science and Engineering*, vol. 10, no. 6, pp. 36-42, 2023. [[CrossRef](#)] [[Publisher Link](#)]

Acknowledgements

The Ministry of Education Malaysia funded this research through Fundamental Research Grant Scheme No. FRGS/1/2020/ICT02/UNIMAP/02/1 and supported by the researchers from University Malaysia Perlis. The authors would like to express their gratitude to the University Malaysia Perlis for their guidance in completing this research study.